Investigation of a high-dose irradiated beryllium microstructure

[1]N.Zimber, [1]P.Vladimirov, [1]M. Klimenkov, [2]V. Kuksenko

[1]Karlsruhe Institute of Technology (KIT), Institute for Applied Materials – Applied Materials Physics (IAM-AWP), Herman-von-Helmholtz-Platz 1, 76344 Eggenstein-Leopoldshafen, Germany

[2]United Kingdom Atomic Energy Authority, Culham Science Centre, Abingdon, Oxfordshire, OX14 3DB, United Kingdom

Corresponding author: Nikolai Zimber

Address: Karlsruhe Institute of Technology (KIT), Institute for Applied Materials – Applied Materials Physics (IAM-AWP), Herman-von-Helmholtz-Platz 1, 76344 Eggenstein-Leopoldshafen, Germany

Telephone number: +49 721 608 28540

E-mail address: nikolai.zimber@kit.edu

Keywords: beryllium, neutron irradiation, TEM, EDX

Graphical Abstract

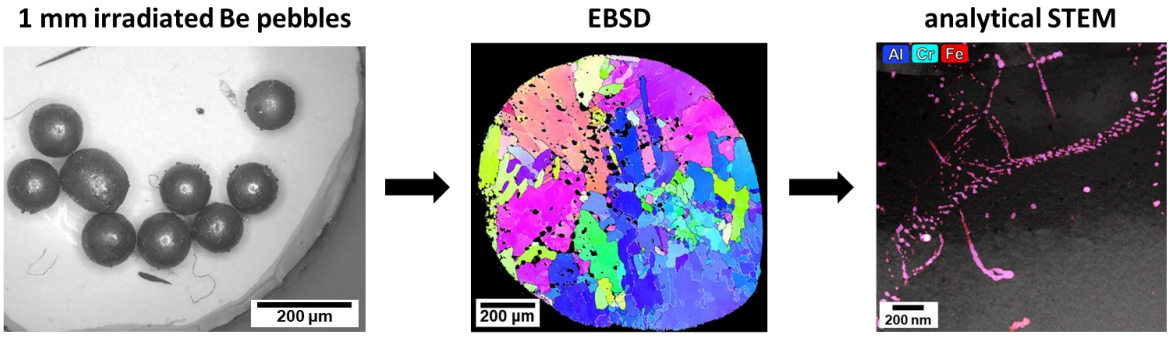

Abstract

The present paper studies the evolving Be microstructure after high-dose neutron irradiation at 660 K, 753 K and 873 K up to 34 dpa and generation of 5524 appm He and 596 appm ^{3}H. At all three temperatures gas bubbles were observed whereby their average size is increasing with the temperature. In addition denuded zones (DZ) formed near grain boundaries. Their width increased with irradiation temperature and was found to be narrower for grains with a random orientation compared to those with a close to basal orientation with respect to the grain boundary. Furthermore, perceptions containing elements such as Al, Cr, Fe, Mg, Si as well as U were found inside single grains, often attached to dislocation lines, and in the vicinity of grain boundaries, mainly at 660 K and 753 K.

1. Introduction

Beryllium is considered as an effective neutron multiplier material for the Helium-Cooled Pebble-Bed (HCPB) design concept of the tritium-breeding blanket being developed at the Karlsruhe Institute of Technology (KIT) [1,2]. Large amounts of helium and tritium will be generated by neutron-induced transmutation within beryllium [3]. Accumulation of tritium within 300 tons of beryllium pebbles required for the demonstration fusion reactor DEMO could imply severe safety and waste processing issues [4]. In order to assess the tritium inventory, a fundamental understanding of the evolving microstructure during neutron irradiation is necessary.

In the past various studies of neutron irradiated beryllium have been performed [5–10]. However, these irradiations were performed either at low temperatures (< 673 K) [5,9,10] or resulted only in relatively low damage and transmutant gas production [6–8]. The region with both, high temperature (673 K to 873 K) and high neutron fluencies (> 3 x 10^{22} cm^{-2}) relevant for the HCPB blanket was therefore missing up to now. To simulate the fusion conditions with respect to temperature, accumulated damage dose as well as helium and tritium production the irradiation campaign HIDOBE-02 was performed in the High-Flux Reactor (HFR) in Petten. Between 2005 and 2011 various Be pebbles with diameters between 0.5-2 mm were irradiated in 1274 full power days (fpd) in 47 reactor cycles within four-years of irradiation. This has led to a damage of up to 34 dpa and a gas production of 5524 appm He and 596 appm ^{3}H. The HIDOBE-02 campaign is the continuation of the HIDOBE-01 program in which approximately half of the helium and tritium production was achieved. [11] Results of the microstructural investigations of the HIDOBE-01 samples can be found in [12–14].

During the HIDOBE irradiation some of the pebbles were just loosely filled into drums and therefore called *unconstrained* while the other fraction was pressed into containments and therefore called *constrained*. The present paper studies the microstructural evolution of 1 mm constrained Be pebbles after the HIDOBE-02 irradiation campaign. A focus is put on the development of second phase precipitates which were already observed in earlier

publications of irradiated beryllium [9,12] The results of the investigation of the unconstrained pebbles can be found elsewhere [15].

2. Experimental Methods

The investigated 1 mm Be pebbles were fabricated by the NGK Insulators Ltd., Japan using the Rotating Electrode Method (REM). Chemical composition of the pebbles is given in Table 1.

Table 1: Chemical composition of the Be pebbles.

element	content (weight %)
Be	99.5
Fe	0.10
Al	0.07
Mg	0.05
Si	0.03
Cr	<0.01
Co	0.0003
Ni	0.01
Cu	<0.01
Mn	0.007
U	0.0068

The temperatures during the irradiation were measured by thermocouples that were located close to the drums containing the Be pebbles. As the temperatures showed large variations, average temperatures are used in this work. More details about temperature control during this irradiation campaign can be found in [16]. The irradiation parameters are summarized in Table 2. Further information about the damage and gas production calculations are presented in [17].

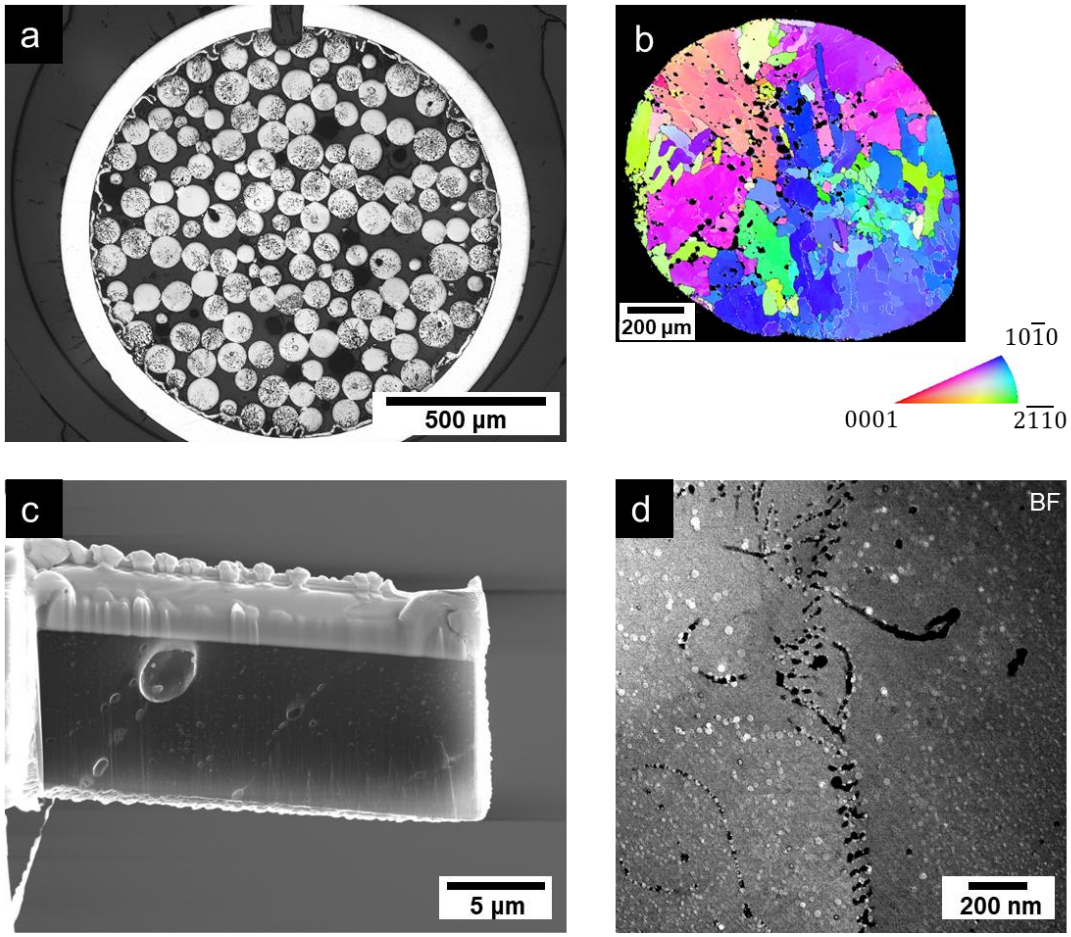

Figure 1: Overview of the TEM-sample preparation: (a) light micrograph of the embedded and mechanically polished pebbles; (b) surface normal-projected inverse pole figure EBSD orientation map of one pebble cross-section, (c) TEM lamella preparation using a FIB; (d) STEM-BF image of a low angle grain boundary.

For the Transmission Electron Microscopy (TEM) sample preparation the irradiated 1 mm pebbles were embedded into epoxy resin and mechanically polished. To gain a first insight into the microstructure of the irradiated Be samples micrographs using a light microscope were acquired (see Figure 1 (a)). A part of more detailed micrographs can be found in [18]. Afterwards electron back scatter diffraction (EBSD) maps (Figure 1 (b)) were obtained in order to identify high- and low angle grain boundaries. TEM lift-outs were then cut from the chosen areas using a FEI Helios Focused Ion Beam (FIB) and thinned to electron transparency using a ZEIS AURIGA (Figure 1 (c)). In order to avoid Be-redepositioning we used relatively high currents (0.5-1 nA) for the main part of the thinning. To obtain a surface that is as free of FIB induced defects as possible thinning was always finished with a 15 min cleaning procedure at 50 pA. Microstructural investigations (Figure 1d) were performed using a FEI Talos F200X TEM operated at 200 kV, equipped with a x-FEG and a Super-X EDX detector with a camera length of 77 mm. For the image acquisition a high-

angle annular dark field (HAADF) and scanning TEM (STEM) bright field (BF) detector were used.

Table 2: Irradiation parameters of 1 mm constrained beryllium pebbles within HIDOBE-02

irradiation temperature (K)			fluence (10^{25} m^{-2})		damage (dpa)	He (appm)	^{3}H (appm)
target	average	maximum	thermal	fast>1 MeV			
678	660	698	7.89	1.6	21	3632	367
773	753	796	9.87	14.3	29	4751	502
893	873	918	11.3	16.8	34	5524	596

3. Results

660 K

The typical microstructure after irradiation at 660 K can be seen in Figure 2 (a). There are many homogeneously distributed bubbles within the grains as well as bubbles directly at the grain boundary (GB). Our recent investigations confirmed the co-existence of helium and tritium within these closed He-bubbles in the grain interior [19]. Since pure vacancy (V) clusters, i.e. voids, cannot exist at GBs as they would dissolve, it is most likely that the voids directly at the GB are also gas filled He-bubbles [20]. At this temperature the average bubble diameter is 23.5 nm.

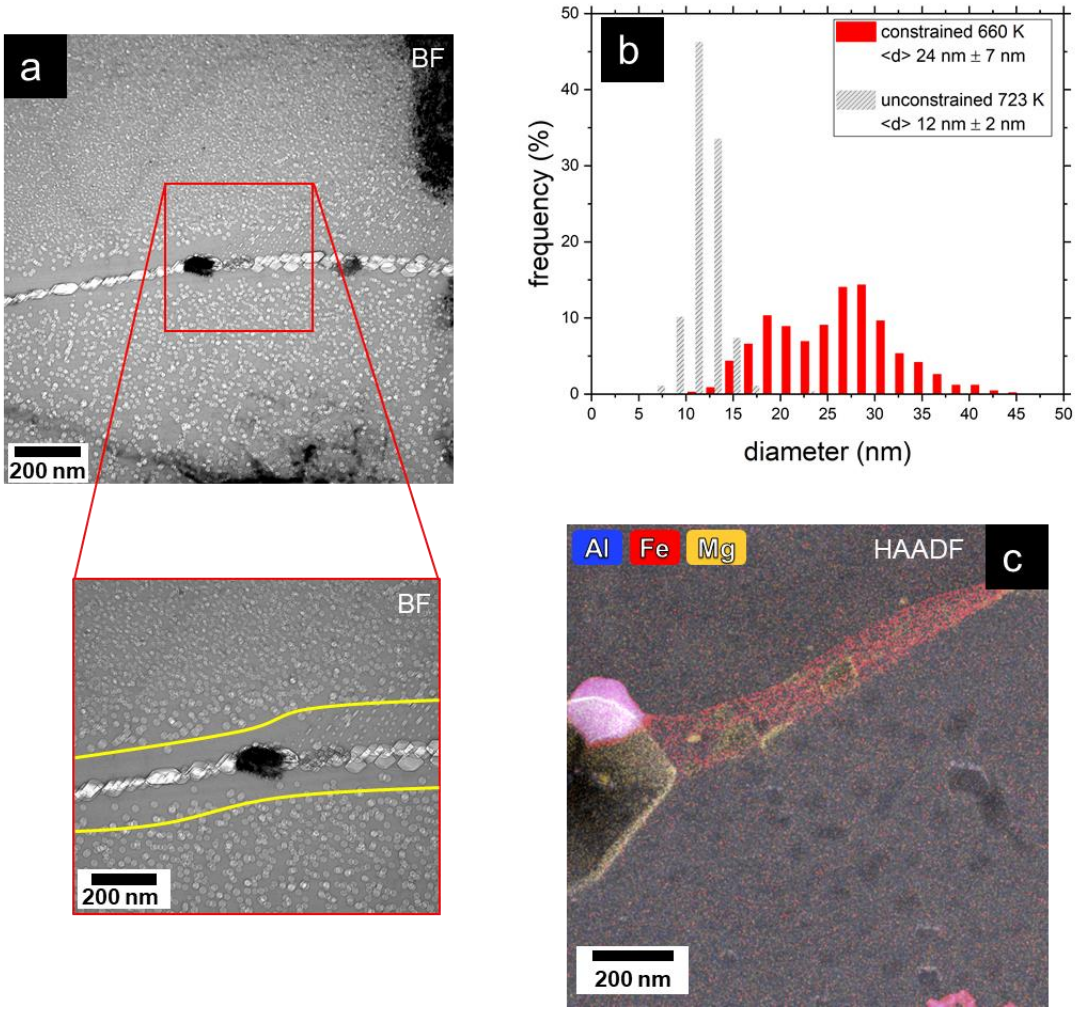

Figure 2: (a) Typical Be microstructure after irradiation at 660 K; (b) corresponding bubble size distribution; (c) segregation of Fe and Mg in the vicinity of a grain boundary.

In earlier investigations, Klimenkov et al. [13] could show with TEM studies of neutron irradiated beryllium, that gas bubbles in beryllium have the shape of a hexagonal prism that was confirmed by our observations. Depending on the orientation of the sample in the TEM either the prismatic faces (Figure 3 (b)) or the hexagonal basal faces (Figure 3 (c)) of the bubble are visible. Appendix 1 shows a tilt series from a close to prismatic orientation to a close to basal orientation by tilting the α angle from -30° to +35°. By having a closer look at Figure 2 (a) it becomes clear, that one can see the hexagonal basal faces of the bubbles. Figure 2 (b) shows the bubble size distribution measured in this work together with the values obtained for the unconstrained samples [15] that were irradiated at similar temperatures. The mean bubble diameter in this work is noticeable larger than for the unconstrained samples. Additionally, the unconstrained pebbles revealed a unimodal bubble size distribution while the bubble size here shows a pronounced bimodal distribution.

In the immediate vicinity of the GBs *bubble denuded zones* (DZ) with no or only very few bubbles are formed. The width of DZs at this temperature is around 50-100 nm and is equal within both grains adjacent to the same GB. In many places, precipitations and segregations of Fe, Al and, sometimes, Mg are formed along GBs as well as within the grains as it can be seen in Figure 2 (c). Whenever Fe and Al were present together they showed a ratio of Fe:Al of exactly or close to 1:1. Usually, precipitates have a size between 50-150 nm.

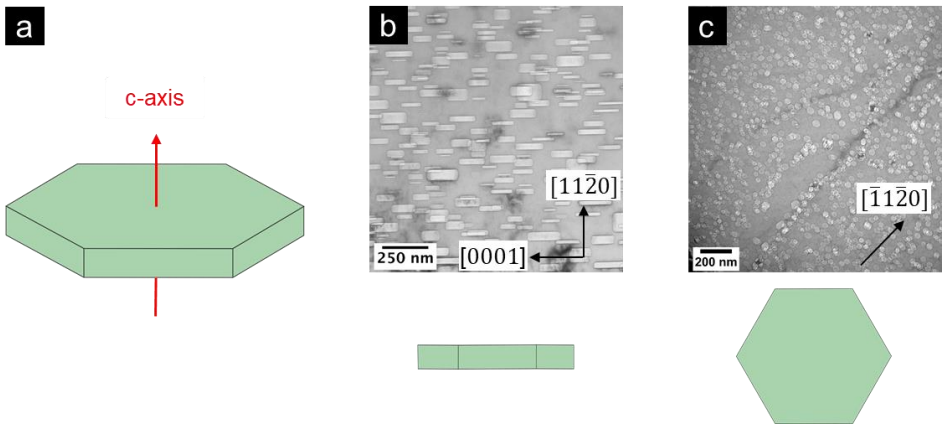

Figure 3: (a) three dimensional model of the bubble shape in beryllium; (b) view on prismatic face; (c) view on basal face

753 K

At 753 K the microstructure is slightly different than at 660 K. DZs have also formed around the GBs. However, these DZs have no longer the same size on both sides of the GBs. As it can be seen from Figure 4 (a) there are large variations in their widths which increased up to 350 nm. At this temperature many precipitates could now be observed in the material whereby the majority of them is attached to dislocation lines and consisted of the Fe-Al enriched phase (purple colour in Figures 4 (c) and 5). As in the case of the 660 K samples, the atomic ratio of Fe:Al was almost every time perfectly 1:1.

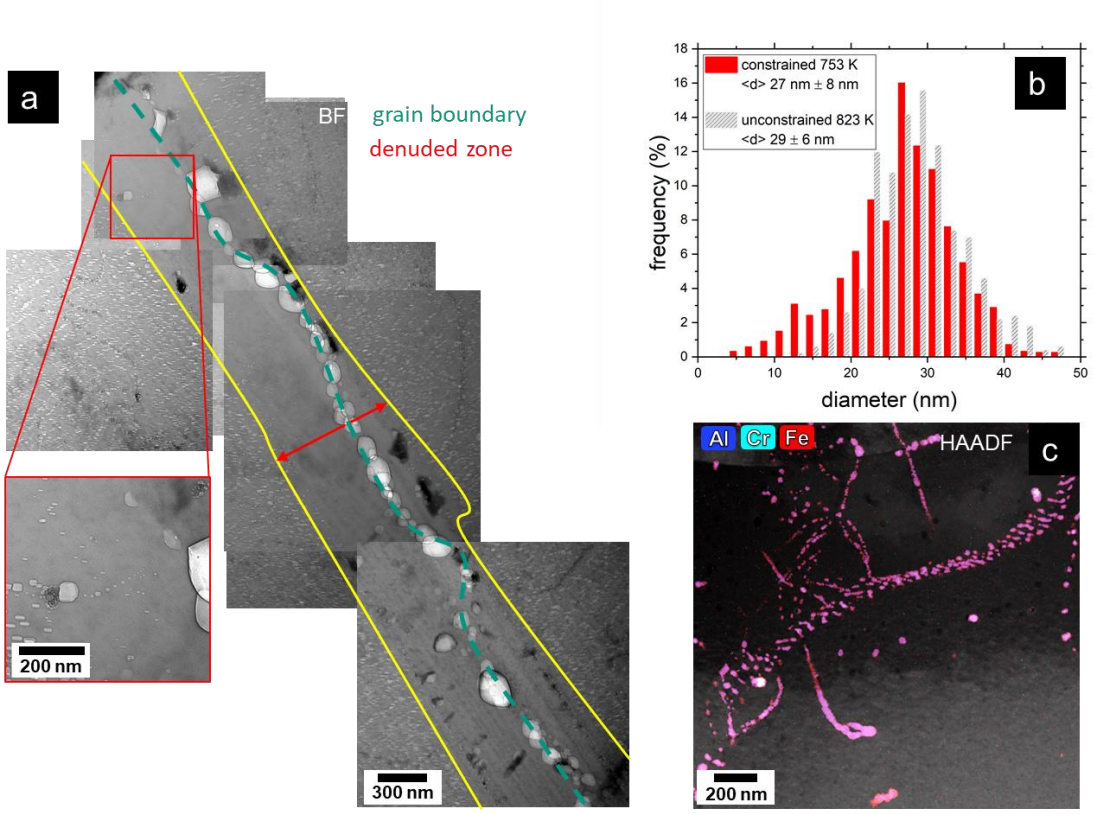

Figure 4: (a) Typical microstructure of Be irradiated at 753 K, the enlarged area shows a chain of bubbles in the DZ; (b) bubble size distribution; (c) low angle GB made up of an array of dislocations decorated with Fe–Al-Be phase precipitates.

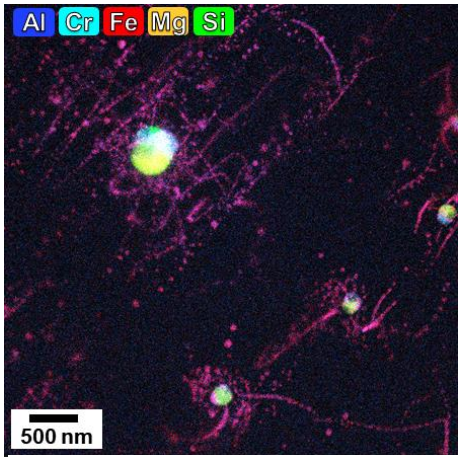

Figure 5. Precipitations in beryllium after neutron irradiation at 753 K.

Figure 4 (c) shows possibly a low-angle GB made up of an array of dislocations that are decorated with iron and aluminium. One has to note that we could never directly observe dislocation lines in Be as they always seem to be decorated with precipitates. In the grain interior also bigger precipitates with sizes up to 300 nm, which are usually complex phase precipitates containing elements such as Al, Si, Cr, Mg and others (see Figure 5) could be observed. Often these precipitates have several shells formed on top of each other. The average bubble diameter is 26.9 nm and therefore almost as large as for the unconstrained samples [15]. The bubble size follows for both sample types a unimodal distribution.

873 K

At the highest irradiation temperature very large bubbles are formed both inside the grains and at GBs (see Figure 6 (a)). In the grain interior, the average bubble diameter is 90 nm,

while directly at the GBs the bubble size even exceeds several 100 nm. Only very few precipitates could be observed after irradiation at 873 K and usually only segregations along GBs as it can be seen from Figure 6 (c) are present. Larger precipitates like the ones in Figure 6 (d) could be observed only rarely, although the Al-Fe-Be phase should, in theory, be stable and present, even at 873 K [21].

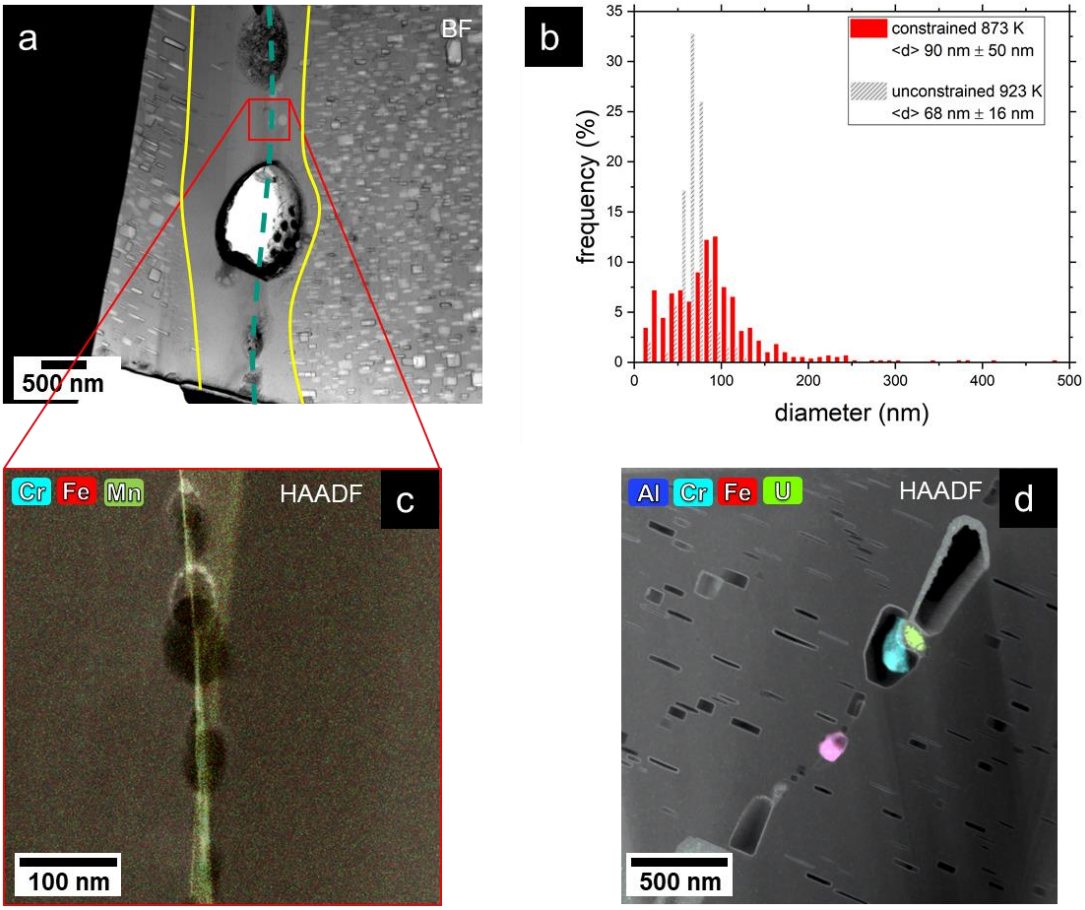

Figure 6: (a) Typical microstructure of Be irradiated at 873 K; (b) bubble size distribution; homogeneous segregation of Cr, Fe and Mn at a GB; (d) precipitates at a GB

At this temperature, no dislocation lines or any indications for them were observed . This can be explained by the fact that in the absence of precipitates, which could pin dislocations, they migrate and form subgrain walls. First evaluation of our EBSD measurements suggest that an increased number of low-angle GBs exist at this temperature. However a more detailed EBSD analysis of this material is necessary to complete the picture. As for the lower irradiation temperatures, DZs are formed in the vicinity of GBs, whereby their size increased up to several micrometres. In comparison to the unconstrained samples [15] which showed a mean bubble size of 68 nm the constrained pebbles in this work showed bubbles with a mean diameter of 90 nm.

Discussion

3.1 Precipitates

In the grain interior bigger precipitates with sizes up to 300 nm could be observed at all three irradiation temperatures. They are usually complex phase precipitates containing natural impurities such as Fe, Al, Si, Cr, Mg and others. These elements have very limited solubility in beryllium and typical precipitate or form segregations in beryllium of industrial purity [22].

As it is indicated in Figure 6 (d), uranium could be found in some places as well. It is known, that this actinide is a natural impurity within some beryllium ores whose concentration should be kept as low as possible due to a possible transmutation into long living, alpha-emitting radioactive isotopes with half-lives greater than 20 years [23,24]. Chemical analysis of our material revealed a U content of < 0.01 wt. ppm.

The majority of all impurity clusters contain Al and Fe (see Figure 4 (c)) as well as Mg and Si (see Figure 2 (c) & Figure 5). It is known that Al and Mg are undesirable contaminants in beryllium as they can lead to hot shortness and a loss of ductility due to segregation at grain boundaries (as observed in Figure 2 (c)) and formation of phases with low melting temperatures [21]. For this reason the content of free aluminium and magnesium should be kept as low as possible, including the eutectically bound one. Mg can be bound by silicon to form a intermetallic phase with a higher melting temperature. For Al this is achieved by doping Be with iron in an Al:Fe ratio of at least 1:2 [21]. According to [21] the following equilibrium is achieved:

$$\begin{array}{ccc} & \overset{< 823\ \mathrm{K}\text{-}1123\ \mathrm{K}}{} & \\ \mathrm{Fe} + \mathrm{Be} + \mathrm{Al} & \rightleftharpoons & \mathrm{AlFeBe_4} \\ \downarrow\uparrow & \underset{> 1123\ \mathrm{K}}{} & \\ \mathrm{FeBe_{11}} & & \end{array} \qquad (1)$$

On the one hand, there is the intermetallic phase $FeBe_{11}$ [25] which has not been observed in this study since every Fe enrich cluster also contained Al. On the other hand, the ternary

compound $AlFeBe_4$ should form between 823 K and 1123 K. However, this phase was only found at the two lower irradiation temperatures. This alleged contradiction can be explained by the radiation-enhanced diffusion [26]: due to an increased number of irradiation-induced defects, the number of possible diffusion paths as well as diffusion rates increases and precipitations form and dissolve at lower temperatures as compared to the equilibrium case.

3.2 Swelling

From the TEM images it is possible to determine volumetric swelling which might have a negative impact if the pebbles lose their structural integrity. Usually [15,18,27] the swelling s_c is calculated as the ratio between the volume of all measured bubbles relative to the volume where they have been measured as it is indicated by equation (2):

$$s_c = \frac{\pi \ < H > \sum_{i=1}^{N} D_i^2}{4V_0} \qquad (2)$$

Here $<H>$ is the mean height of all bubbles, D the perimeter of the hexagon and V_0 the measuring volume. However, since the displacement damage as well as the helium production varies with the temperature for neutron irradiation experiments it might be appropriate to account for that and scale the swelling to the dpa as it is shown in equation (3). This expression also ensures that the swelling is calculated relative to the initial volume V_0 and not, as it is done often in the literature [15,18,27], to the final volume V which is not correct for larger swelling values. In order to determine V_0 the thickness of the lamellae were measured using the electron energy loss spectroscopy (EELS) log-ratio technique.

$$S = \frac{\left(\frac{s_c}{1 - s_c}\right)}{\text{dpa}} \qquad (3)$$

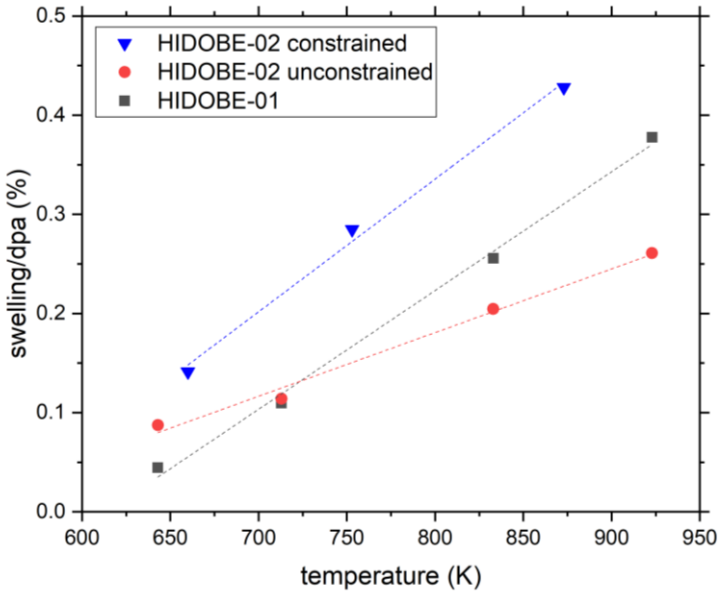

Figure 7: Swelling/dpa for different Be samples.

In Figure 7 the swelling/dpa as a function of temperature is plotted together with the values measured on other Be samples irradiated in HIDOBE irradiation campaign [15,18]. On the one hand, the swelling/dpa increases linear with the temperature for different types of Be samples with nearly the same slope. On the other hand, the swelling remains relatively low, i.e. < 0.5 %/dpa for all three investigated temperatures.

3.3 Denuded Zone

At all three irradiation temperatures the formation of DZs could be observed in the immediate vicinity of GBs. While the sizes of the DZs were comparable on both sides of the GBs at 660 K, there were strong variations at 753 K and 873 K. In the past many investigations have been performed aiming at connection of the DZ formation with the grain boundary character [28–35]. Usually the misorientation angle between two grains is taken to describe the GB character in the aforementioned publications. However, the literature is not consistent weather or not the width of the DZ is really influenced by the misorientation angle. This is most likely due to the fact that the misorientation angle is only one of five parameters that are necessary to fully describe a GB [36,37]. Besides the three rotation or Eularian angles two parameters to define the boundary plane by its Miller indices are needed. Although it is possible to fully characterize a GB in the TEM [38], to our knowledge this has never been done at grain boundaries with DZs. Most likely because procedures like the one described in [38] are very time consuming and it is difficult to apply them for heterogeneous material systems.

Since GBs are strong sinks for point defects, the vacancy concertation, or in our case rather the concentration of HeV-cluster since He is strongly bound to vacancies [39], is visibly lower in the vicinity of the GBs than in the grain interior. The difference in the HeV concentration creates a concentration gradient that leads to a vacancy migration to the GB.

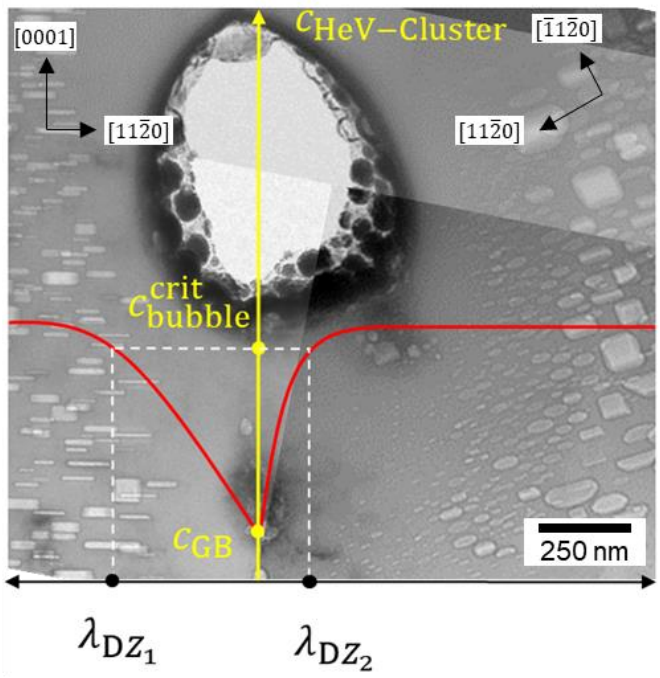

As soon as steady state is reached the concentration of HeV-clusters increases from the GB to the grain interior as it is shown in Figure 8. If one assumes that bubbles or cavities can only form above a critical HeV-concentration a bubble denuded zone is formed. The DZ in the left grain of Figure 8 is almost three times larger than the one in the right grain. In addition it can be seen that the bubbles in the left grain show a basal orientation.

Figure 8: DZ formation in Be after irradiation at 873 K; marks the critical HeV-cluster concentration that is necessary for bubble nucleation.

Following Beyerlein et al. [40] the DZ width can be expressed by equation 3:

$$\lambda_{\mathrm{DZ}} = \left(\ln \eta_{\mathrm{HeV}} - \ln \left(1 - \Delta c^{*}_{\mathrm{HeV}} \frac{K_{\mathrm{SHeV}}}{K_0} \right) \right) \sqrt{\frac{D_{\mathrm{HeV}}}{K_{\mathrm{SHeV}}}} \qquad (3)$$

where λ_{DZ} is the width of the denuded zone, η_{HeV} is the HeV-cluster sink efficiency, $\Delta c^{*}_{\mathrm{HeV}}$ the critical HeV-cluster concentration necessary for nucleation of gas bubbles, K_{SHeV} the HeV-cluster-sink reaction rate coefficient, K_0 the deffect production rate and D_{HeV} the HeV-cluster diffusivity. Our previous simulations have shown that He and HeV-cluster diffuse faster along the basal planes than perpendicular to these planes [39]. This makes it clear why the width λ_{DZ_1} of the DZ for basal oriented grain on the left is larger than the size on the right hand side where basal plane has smaller angle with the GB plane: The HeV clusters seem to escape to the GB much more effectively in grains that are oriented so that the basal plane is perpendicular to the GB plane. However, as mentioned earlier in this paper, the misorientation is only one of five parameters and the other four might also play an important role in the DZ formation.

Interestingly enough, at some places one could observe again and again chains of bubbles in the DZs (see enlarged area in Figure 4 (a)). First of all this observation is contradictory,

since it is commonly assumed that the DZ is only formed because GBs are strong sinks for point defects and the vacancy- and gas-concentration in their immediate vicinity is too low for bubble formation. Therefore it can be concluded that these bubbles have grown along dislocation lines that were trapped at grain boundaries and that provided the necessary vacancies for bubble nucleation and growth

4. Conclusion

In the present paper the microstructural changes in beryllium irradiated with neutrons at three different temperatures was studied in TEM. The main finding of these investigations can be summarized as follows.

(1) Bubbles formed at all three irradiation temperatures whereby their size increased with temperature from 24 nm at 660 K to 90 nm at 873 K.
(2) At all three irradiation temperatures bubble DZs formed along GBs whereby their width is increasing with the temperature up to a size of several microns at 873 K.
(3) The width of the DZs showed a strong correlation with the grain orientation as the diffusion coefficient of HeV-cluster is higher along the basal planes then perpendicular to them
(4) Chains of bubbles were found in the DZ. These chains are possibly aligned along dislocation lines attached to the GBs.
(5) Precipitates and segregations of elements such as Al, Fe, Cr, Mg, Si and U were predominantly observed after irradiation at 660 K and 753 K.

Appendix

Appendix 1: bubble tilt series from a close to prismatic orientation to a close to basal orientation by tilting the α angle from -30° to +35°.

Authors Contributions

V.K. performed the EBSD analysis and the FIB lift-outs. N.Z. thinned the lamellae to electron transparency and performed the microstructural TEM investigations and the associated data analysis. P.V. and M.K. provided guidance on the result analysis. N.Z. wrote the manuscript with input from all authors.

Acknowledgment

This work has been carried out within the framework of the EUROfusion Consortium and has received funding from the Euratom research and training programme 2014-2018 and 2019-2020 under grant agreement No 633053. The views and opinions expressed herein do not necessarily reflect those of the European Commission.

The research used FIB from the UKAEA's Materials Research Facility, which has been funded by and is part of the UK's National Nuclear User Facility and Henry Royce Institute for Advanced Materials. V.K. contribution work was also partially funded by the RCUK Energy Programme (Grant No. EP/T012250/1).

Data availability

The datasets generated during and/or analysed during the current study are available from the corresponding author on reasonable request.

5. References

[1] F. Hernández, P. Pereslavtsev, Q. Kang, P. Norajitra, B. Kiss, G. Nádasi, O. Bitz, A new HCPB breeding blanket for the EU DEMO: Evolution, rationale and preliminary performances, Fusion Engineering and Design 124 (2017) 882–886.

[2] F.A. Hernández, P. Pereslavtsev, G. Zhou, B. Kiss, Q. Kang, H. Neuberger, V. Chakin, R. Gaisin, P. Vladimirov, L.V. Boccaccini, G.A. Spagnuolo, S. D'Amico, I. Moscato, Advancements in the Helium-Cooled Pebble Bed Breeding Blanket for the EU DEMO: Holistic Design Approach and Lessons Learned, Fusion Science and Technology 75 (2019) 352–364.

[3] F. Scaffidi-Argentina, Modellierung des Schwellens und der Tritium-Freisetzung von bestrahltem Beryllium: FZKA 5632, 1995.

[4] M. Dalle Donne, H. Albrecht, L.V. Boccaccini, F. Dammel, U. Fischer, H. Gerhardt, K. Kleefeldt, W. Nägele, P. Norajitra, G. Reimann, H. Reiser, O. Romer, P. Ruatto, F. Scaffidi-Argentina, K. Schleisiek, H. Schnauder, G. Schumacher, H. Tsige-Tamirat, B. Tellini, P. Weimar, A. Weisenburger, H. Werle, European DEMO BOT solid breeder blanket, Karlsruhe, 1994.

[5] V.P. Chakin, Z.Y. Ostrovsky, Evolution of beryllium microstructure under high-dose neutron irradiation, Journal of Nuclear Materials 307-311 (2002) 657–663.

[6] E Rabaglino, C Ferrero, J Reimann, C Ronchi, T Schulenberg, Study of the microstructure of neutron irradiated beryllium for the validation of the ANFIBE code, Fusion Engineering and Design 61-62 (2002) 769–773.

[7] D.S. Gelles, H.L. Heinisch, Neutron damage in beryllium, Journal of Nuclear Materials 191-194 (1992) 194–198.

[8] I.B. Kupriyanov, V.A. Gorokhov, R.R. Melder, Z.E. Ostrovsky, A.A. Gervash, Investigation of ITER candidate beryllium grades irradiated at high temperature, Journal of Nuclear Materials 258-263 (1998) 808–813.

[9] V. Kuksenko, K. Ammigan, B. Hartsell, C. Densham, P. Hurh, S. Roberts, Irradiation effects in beryllium exposed to high energy protons of the NuMI neutrino source, Journal of Nuclear Materials 490 (2017) 260–271.

[10] L. Sannen, C. de Raedt, F. Moons, Y. Yao, Helium content and induced swelling of neutron irradiated beryllium, Fusion Engineering and Design 29 (1995) 470–474.

[11] J.B.J. Hegeman, J.G. van der Laan, H. Kawamura, A. Möslang, I. Kupriyanov, M. Uchida, K. Hayashi, The HFR Petten high dose irradiation programme of beryllium for blanket application, Fusion Engineering and Design 75-79 (2005) 769–773.

[12] M. Klimenkov, V. Chakin, A. Moeslang, R. Rolli, TEM study of impurity segregations in beryllium pebbles, Journal of Nuclear Materials 455 (2014) 660–664.

[13] M. Klimenkov, V. Chakin, A. Moeslang, R. Rolli, TEM study of beryllium pebbles after neutron irradiation up to 3000appm helium production, Journal of Nuclear Materials 443 (2013) 409–416.

[14] Klimenkov Michael, Hoffmann Jan, Kurinsky Peter, Kuksenko Viacheslav, Vladimirov Pavel, Chakin Vladimir, Möslang Anton, TEM characterization of irradiated beryllium, in: European Microscopy Congress 2016: Proceedings, American Cancer Society, 2016, pp. 880–881.

[15] M. Klimenkov, P. Vladimirov, U. Jäntsch, V. Kuksenko, R. Rolli, A. Moeslang, N. Zimber, New insights into microstructure of irradiated beryllium based on experiments and computer simulations, Scientific reports (accepted manuscript) (2020).

[16] S. van Til, A. Sugonyako, HIDOBE: final report on irradiation up to 3000 appm He, NRG-20296/09.96239/P,TW2-TTBB-004b D4b (2009).

[17] B.T. Straathof, HIgh DOse Irradiation of BEryllium - HIDOBE 02 (351-02), NRG-23388/16.140801 (2016).

[18] M. Zmitko, P. Vladimirov, R. Knitter, M. Kolb, O. Leys, J. Heuser, H.-C. Schneider, R. Rolli, V. Chakin, S. Pupeschi, L. Magielsen, A. Fedorov, Y. Poitevin, Development and qualification of functional materials for the European HCPB TBM, Fusion Engineering and Design 136 (2018) 1376–1385.

[19] M.S. Blackmur, S. Dumbill, I. MacLaren, D. Hernandez-Maldonado, P.D. Styman, M. Gass, R.J. Nicholls, J.M. Hyde, Q.M. Ramasse, K.J. Annand, J.S. Smith, N. Gotham, The association of hydrogen with nanometre bubbles of helium implanted into zirconium, Scripta Materialia 152 (2018) 102–106.

[20] B.N. Singh, A.J.E. Foreman, Relative role of gas generation and displacement rates in cavity nucleation and growth, Journal of Nuclear Materials 122 (1984) 537–541.

[21] K.A. Walsh, E.E. Vidal, Beryllium chemistry and processing, ASM International, Materials Park,Ohio, 2009.

[22] D.R. Floyd, J.N. Lowe, Beryllium Science and Technology, Springer US, Boston, MA, 1979.

[23] Glen R. Longhurst, Beryllium Use in the Advanced Test Reactor (2007).

[24] C.B.A. Forty, R.A. Forrest, G.J. Butterworth, Activation of beryllium in a fusion power plant, Journal of Nuclear Materials 258-263 (1998) 793–797.

[25] O.K. von Goldbeck, Fe—Be Iron—Beryllium, in: O.K. von Goldbeck (Ed.), IRON—Binary Phase Diagrams, Springer Berlin Heidelberg, Berlin, Heidelberg, 1982, pp. 18–22.

[26] W. Gary S., Fundamentals of Radiation Materials Science: Metals and Alloys, Springer Berlin Heidelberg, Berlin, Heidelberg, 2007.

[27] P. Liu, Q. Zhan, W. Hu, Y. Jia, W. Han, X. Yi, F. Wan, Microstructure evolution of beryllium with argon ion irradiation, Nuclear Materials and Energy 13 (2017) 99–103.

[28] P.A. Thorsen, J.B. Bilde-Sørensen, B.N. Singh, Bubble formation at grain boundaries in helium implanted copper, Scripta Materialia 51 (2004) 557–560.

[29] W.Z. Han, M.J. Demkowicz, E.G. Fu, Y.Q. Wang, A. Misra, Effect of grain boundary character on sink efficiency, Acta Materialia 60 (2012) 6341–6351.

[30] O. El-Atwani, J. A. Hinks, G. Greaves, J. P. Allain, S. A. Maloy, Grain size threshold for enhanced irradiation resistance in nanocrystalline and ultrafine tungsten, Materials Research Letters 5 (2017) 343–349.

[31] O. El-Atwani, J.E. Nathaniel, A.C. Leff, B.R. Muntifering, J.K. Baldwin, K. Hattar, M.L. Taheri, The role of grain size in He bubble formation: Implications for swelling resistance, Journal of Nuclear Materials 484 (2017) 236–244.

[32] Y. Sekio, S. Yamashita, N. Sakaguchi, H. Takahashi, Void denuded zone formation for Fe–15Cr–15Ni steel and PNC316 stainless steel under neutron and electron irradiations, Journal of Nuclear Materials 458 (2015) 355–360.

[33] C.M. Barr, L. Barnard, J.E. Nathaniel, K. Hattar, K.A. Unocic, I. Szlurfarska, D. Morgan, M.L. Taheri, Grain boundary character dependence of radiation-induced segregation in a model Ni–Cr alloy, J. Mater. Res. 30 (2015) 1290–1299.

[34] X.M. Bai, A.F. Voter, R.G. Hoagland, M. Nastasi, B.P. Uberuaga, Efficient Annealing of Radiation Damage Near Grain Boundaries via Interstitial Emission, Science 327 (2010) 1631–1634.

[35] O. El-Atwani, J.E. Nathaniel, A.C. Leff, K. Hattar, M.L. Taheri, Direct Observation of Sink-Dependent Defect Evolution in Nanocrystalline Iron under Irradiation, Scientific reports 7 (2017) 1836.

[36] Saylor, David M. and El-Dasher, Bassem S. and Adams, Brent L. and Rohrer, Gregory S., Measuring the five-parameter grain-boundary distribution from observations of planar sections, Metallurgical and Materials Transactions A 35 (2004) 1981–1989.

[37] Valerie Randle, A methodology for grain boundary plane assessment by single-section trace analysis, Scripta Materialia 44 (2001) 2789–2794.

[38] Á.K. Kiss, E.F. Rauch, B. Pécz, J. Szívós, J.L. Lábár, A Tool for Local Thickness Determination and Grain Boundary Characterization by CTEM and HRTEM Techniques, Microscopy and Microanalysis 21 (2015) 422–435.

[39] P.V. Vladimirov, A. Moeslang, Ab initio static and molecular dynamics studies of helium behavior in beryllium, Journal of Nuclear Materials 442 (2013) S694-S698.

[40] I.J. Beyerlein, M.J. Demkowicz, A. Misra, B.P. Uberuaga, Defect-interface interactions, Progress in Materials Science 74 (2015) 125–210.